Applied Materials Today 47 (2025) 102978

Contents lists available at ScienceDirect

Applied Materials Today

journal homepage: www.elsevier.com/locate/apmt

Hyaluronic acid-*g*-poly(lactic acid) and poly(vinyl alcohol) inks for 3D printed berberine loaded foldable dressings

Nicola Filippo Virzì [a,b], Carmen Alvarez-Lorenzo [b], Angel Concheiro [b], Veronica Casagranda [c], Valeria Pittalà [a,*], Patricia Diaz-Rodriguez [b,*]

[a] Department of Drug and Health Science, University of Catania, Viale A. Doria 6, 95125 Catania, Italy
[b] Departamento de Farmacología, Farmacia y Tecnología Farmacéutica, I+D Farma (GI-1645), Faculty of Pharmacy, Instituto de Materiales (iMATUS), and Health Research Institute of Santiago de Compostela (IDIS), Universidade de Santiago de Compostela, 15782 Santiago de Compostela, Spain
[c] Novagenit Srl, Via Trento, 115, 38017 Mezzolombardo, Trento, Italy

ARTICLE INFO

Keywords:
Hyaluronic acid
Poly(lactic acid)
Poly(vinyl alcohol)
3D printing
Wound dressing
Berberine

ABSTRACT

Antimicrobial resistance (AMR) has increased the urgency for novel wound care strategies. Semi Solid Extrusion (SSE)-3D printing technology holds significant promise in this area, allowing for the creation of personalized and customizable wound dressings. This study focused on developing a foldable and flexible dressing capable of incorporating and releasing non-antibiotic antimicrobial compounds, such as berberine (Ber). To this end, a hyaluronic acid (HA)-g-poly(lactic acid) (PLA)-based polymer (DAC®) was combined with poly(vinyl alcohol) (PVA) to enhance the mechanical properties and foldability of 3D-printed dressings. On the other hand, propylene glycol (PG) was incorporated to facilitate the integration of non-water soluble natural antimicrobial compounds like berberine (Ber). The rheological profile of DAC/PVA/PG blends was optimized for 3D printing, resulting in printing-compatible inks. After freeze-drying, a sterilization/crosslinking process through autoclave allowed to reduce dressings swelling (~98 % less in simulated wound fluid and ~ 99 % less in water), suitable to preserve their foldability without losing structural shape, while improving mechanical properties (from 1.74 MPa to 2.85 MPa tensile strength). The antimicrobial efficacy of Ber-loaded dressings against *Staphylococcus aureus* was demonstrated by microcalorimetry, although the incorporation of Ber did not significantly enhance antibiofilm activity when compared to blank dressings. *In vitro* cytotoxicity tests confirmed that over 70 % of human dermal fibroblasts remained viable after 24 h of exposure to the Ber-loaded dressings. This work suggests the chosen polymer combination is promising to produce flexible and foldable dressings that can be adapted to anatomically complex wounds. The loading of natural antimicrobial agents, such as Ber, holds potential for addressing infected wounds as an alternative to traditional treatments in the face of AMR.

1. Introduction

Wound management remains a critical challenge in the clinic, particularly considering the growing threat posed by antimicrobial resistance (AMR) [1]. Infected wounds, particularly those in patients with comorbidities such as diabetes, immunodeficiency, or vascular disease, are at high risk for complications, including sepsis, gangrene, or limb amputation [2]. The growing prevalence of AMR requires the development of novel therapeutic strategies that can both combat infections and facilitate wound healing, without solely relying on traditional antibiotics.

Widely used passive dressings such as gauzes, cotton pads, and bandages are no longer sufficient to meet the current clinical needs. These materials primarily serve as barriers, offering basic protection against contaminants and aiding in fluid absorption. While they are cost-effective and readily available, they do not actively contribute to the healing process [3]. Moreover, they often adhere to the wound surface, potentially causing additional tissue damage and pain upon removal. To overcome these limitations, a range of advanced wound care materials and active dressings, such as hydrogels, films, foams, and sponges, have been introduced in clinical practice. These are specifically designed to create a more favourable wound environment by regulating moisture, promoting oxygen exchange, and, in some cases, delivering bioactive molecules in a controlled and localized manner able to induce healing

* Corresponding authors.
E-mail addresses: valeria.pittala@unict.it (V. Pittalà), patricia.diaz.rodriguez@usc.es (P. Diaz-Rodriguez).

https://doi.org/10.1016/j.apmt.2025.102978
Received 2 June 2025; Received in revised form 21 October 2025; Accepted 24 October 2025
Available online 31 October 2025

[4].

The use of 3D printing in wound care has garnered attention due to its ability to produce personalized and customizable wound dressings with precise control over shape, size, and material properties. This feature is particularly advantageous for the treatment of complex wounds, such as those found with irregularly shape or anatomically challenging areas [5]. 3D printed dressings can replicate the tissue architecture, create gas and nutrients permeable structures, control moisture, and allow drug release, which can *in toto* contribute to creating an optimal microenvironment for wound healing thus offering a promising path toward more effective, adaptable, and patient-centered wound care solutions [6].

Among the existing techniques, Semi Solid Extrusion (SSE) is an election technique for fabricating 3D hydrogel-based scaffolds with controlled architecture, organized porosity, and high reproducibility [7]. When suitable materials are used, such as polysaccharides, SSE can produce biocompatible and biodegradable wound dressings. Moreover, it offers several benefits, including efficient exudate absorption, moisture retention, gas exchange, cell attachment, and pro-regenerative properties [8,9].

However, one of the main challenges in SSE-3D printing of polysaccharide-based materials lies in the production of flexible wound dressings. While SSE-3D printing technology is well-suited for fabricating rigid or semi-rigid structures, producing foldable and flexible devices that maintain their functionality is considerably more challenging [10]. Indeed, polysaccharides usually generate devices that, especially after drying or freeze-drying, present high brittleness and no possibility to be folded without breaking or damaging the original shapes [11,12].

To overcome these limitations, recent advances in 3D printing have been focused on developing mechanically robust and elastic hydrogels capable of mimicking soft and flexible biological tissues [13]. These approached comprise the formation of double-network (DN) hydrogels and nanofibrillar-based or nanocomposite hydrogels [13]. DN hydrogels combine two interpenetrating polymer networks to achieve strength and elasticity. A clear example is Fe^{3+}-crosslinked sodium alginate/poly (acrylamide-co-acrylic acid) DN hydrogel, that allowed successful 3D printing into complex constructs depicting flexibility, stretchability, and improved toughness [14]. On the other hand, nanofibers can reinforce the polymer matrix, improving final material properties. Indeed, alginate/nanocellulose hydrogels have been developed as 3D-printable materials for the production of soft and conformable wound dressings [15]. Furthermore, the use of Cellulose nanofibrils (CNFs) in Direct Ink Writing (DIW) approach have been reported as proficient strategy for creating strong and ductile films [16]. Collectively, these strategies illustrate the necessity of enhancing the mechanical resilience and foldability of 3D-printed polysaccharide-based constructs, which remains a key design challenge.

Foldability is a key attribute for wound dressings that have to fit to the irregular shape and topography of the wound site, improving the dressing's contact with the wound bed and ensuring more consistent therapeutic effects [17]. This issue is particularly important in areas with anatomical complexities, such as joints or concave areas, where rigid dressings may fail to adhere properly or provide adequate coverage. Moreover, rigid dressings can be uncomfortable, especially in high-mobility areas where the dressing may cause friction or pressure on the wound. Moreover, finding materials for 3D printing that can exhibit pro-wound healing features, biocompatibility, and flexibility at the same is not trivial. Indeed, the ability to design a dressing that retains its foldability over time, withstanding the mechanical stresses associated with wound healing while promoting wound closure, requires precise control over the material properties.

Hyaluronic acid (HA), a naturally occurring glycosaminoglycan, plays a crucial role in tissue repair and regeneration. As a major component of the extracellular matrix, HA is involved in processes such as cell migration and angiogenesis [18,19]. Particularly, HA has been shown to accelerate the inflammatory phase of wound healing, promote the formation of granulation tissue, and enhance epithelialization, which is crucial for wound closure [20]. HA's hydrophilic nature maintains moisture at the wound site, preventing dehydration and creating a favourable environment for cellular activities [21]. Furthermore, HA's ability to modulate the immune response and promote collagen synthesis makes it an ideal candidate for use in 3D-printed wound dressings, where its inclusion can accelerate tissue regeneration and reduce scarring [22].

In the present work, a commercially available copolymer of HA grafted with poly(lactic acid) (PLA) called DAC® [23] was evaluated, for first time, for the development of foldable 3D printed wound dressing. DAC® is obtained by grafting PLA onto the HA chains and used in clinics as a peri-operative wet coating for prosthesis to prevent Periprosthetic Joint Infections (PJI) [24]. Owning viscoelastic rheological behaviour, DAC® can be an interesting source for ease HA supply and applications in 3D printing, although its use is currently limited to solid supports coatings [25]. Therefore, foldability properties are unknown. On the other hand, poly(vinyl alcohol) (PVA), a synthetic water-soluble polymer, is often used to create foldable films that can provide a moist environment. PVA is biocompatible, non-toxic, and biodegradable, which makes it suitable for various applications in the pharmaceutical field. Its ability to form strong, flexible, and non-toxic films can be of interest to control and enhance the foldability of other materials [26]. Moreover, the incorporation of propylene glycol (PG) into the ink could allow the loading of hydrophobic natural antimicrobial compounds, widening the applicability of the dressing also for infected wounds. Indeed, the hypothesis of the present work is that a blend of DAC®, PVA and PG can produce a semi-elastic, foldable, and berberine (Ber) containing SSE-3D printed wound dressing.

Ber was selected as therapeutic molecule due to its proven antibacterial efficacy against a broad spectrum of clinically relevant pathogens, many of which are common causes of wound infections [27–29]. Natural alkaloid compounds found in plants, as Ber, other than displaying a wide range of biological activities, including anticancer, anti-inflammatory, antidiabetic, antipyretic, and antibacterial properties, can present several advantages in the fight against antimicrobial resistance (AMR) [30,31]. Their inherent structural complexity and diverse chemical scaffolds enable interactions with multiple bacterial targets, leading to distinct and multitarget mechanisms of action that can overcome bacterial defense systems and reduce the likelihood of resistance development [30,32]. Furthermore, these compounds tend to exert lower selective pressure on bacterial populations compared to traditional antibiotics, which may slow the emergence of resistance and can act synergistically with existing antibiotics, enhancing their efficacy against resistant strains [33]. Moreover, due to their multifaceted nature, these compounds may offer several therapeutic effects simultaneously, such as antibacterial and antioxidant actions [34].

On the other hand, encapsulating high doses of hydrophobic natural compounds, such as Ber, into hydrogel-based inks, like those used in SSE 3D printing, presents a significant challenge for clinical application. Developing strategies to overcome these loading limitations could pave the way for the broader use of compounds with promising therapeutic potential [35].

Although the minimum inhibitory concentrations (MICs) of natural compounds are often higher than those of conventional antibiotics, this does not necessarily limit their therapeutic value. Particularly in the context of multidrug-resistant pathogens, compounds with moderate antimicrobial activity may contribute significantly by acting through mechanisms distinct from existing drugs or by resensitizing resistant bacteria [36]. Overall, Ber antimicrobial properties justify its further investigation as a potential agent in wound healing and AMR management. Importantly, many natural compounds, such as Ber, have demonstrated favourable safety profiles in clinical and traditional medicine settings, supporting their potential for clinical translation [37].

To carry out the work, DAC/PVA/PG blends were designed and tested regarding rheological properties. Ber was loaded thanks to the PG presence into the blend. The formulated ink was used to print squared shaped wound dressings, which were freeze-dried and subsequently crosslinked by an in-autoclave sterilization/crosslinking process. After production, the patches were extensively characterized in terms of swelling ability, mechanical properties, ATR-FTIR analysis, antimicrobial and antibiofilm performance against *Staphylococcus aureus*, together with *in vitro* cytotoxicity assessments.

2. Materials and methods

2.1. Materials

DAC® (Defensive Antibacterial Coating, HA-g-PLA, batch U90183, powder, viscosity 800 Pa•s at 6 % w/v, grafting degree % (expressed as: (moles PLA chains/moles of HA repeating units) × 100) 7 ± 1 mol % [38]) was gifted by Novagenit S.r.l. (Mezzolombardo, Italy). PVA (Mw 89,000–98,000, 99+ % hydrolyzed), propylene glycol (PG, >99 %), thymol (Thy, >99 %), vancomycin (Van, >99 %), gallic acid (GA, >99 %) were obtained from Sigma Aldrich (Darmstadt, Germany), berberine hydrochloride (Ber, >99 %) was provided by TCI Europe (Zwijndrecht, Belgium). Phosphate buffer saline (PBS), TrypLE®, Dulbecco's Modified Eagle Medium (DMEM), Gibco™ Antibiotic-Antimycotic, FBS and Alamar Blue™ were purchased from ThermoFisher Scientific (Waltham, USA). Simulated Wound Fluid (SWF) was prepared with 8.298 g of NaCl and 0.368 g of $CaCl_2$ *per* liter of double distilled water (DDW). Tryptic soy broth (TSB) was purchased from Oxoid (Hampshire, UK), Bacto™ yeast and Bacto™ tryptone extract were obtained from Becton, Dickinson and Company (Le Pont de Claix, France). *S. aureus* ATCC 25,923 was purchased from (ATCC, Manassas, USA).

2.2. Hydrogels and ink formulation

A two-syringe mixture method was used for the preparation of DAC® at 1, 3, and 6 % w/v hydrogels. DAC® powder was weighed and inserted into one syringe, while the required amount of DDW was inserted into another syringe. The syringe was connected by luer-lock connector, and the content was mixed until obtaining a homogenized hydrogel.

To prepare the PVA 6.6 % w/v dispersion, 1 g of PVA was added to a 20 mL glass vial containing 15 mL of DDW. Then the vial was sealed, and the dispersion was vigorously stirred at 90 °C for 1.5 h. The PVA dispersion was cooled down at room temperature (r.t) before use.

Ink formulations (P1, P2, P3 and P1-Ber) with the compositions reported in Table 1 were prepared. The DAC® powder was weighed and placed in a syringe, and an appropriate amount of PG (or PG solution containing Ber) was then added to the syringe containing the powder. Then, the syringe was connected to another one with an appropriate amount of PVA 6.6 % w/v solution (and additional DDW for P3) and mixed until the formation of a homogenized hydrogel.

Table 1
Composition of the DAC® hydrogels and inks (1 mL), and code names of the obtained dressings. DDW was used as dispersant.

Sample	DAC (mg)	PVA 6.6 % w/v (mL)	PG (mL)	H_2O (mL)	Ber (mg, dissolved in PG)	Obtained dressing name
DAC 1 %	10	–	–	1		–
DAC 3 %	30	–	–	1		–
DAC 6 %	60	–	–	1		–
P1	30	0.7	0.3	–		Blank-P
P2	30	0.9	0.1	–		
P3	39	0.7	0.3	0.3		
P1-Ber	30	0.7	0.3	–	5	Ber-P

2.3. Rheology

The rheological behaviour and self-healing properties of the inks were assessed through mechanical testing using an Anton Paar MCR 302 rheometer (Graz, Austria), equipped with a HPTD 200 Peltier hood and a disposable aluminium parallel measuring plate (15 mm in diameter). The measurements were conducted at a constant temperature of 20 °C and performed in triplicate. A fixed gap of 1 mm was maintained throughout the experiment. The test involved a five-step amplitude sweep mode, conducted at a constant frequency of 1 Hz, following a previously established procedure [39–41]. The five steps included: 0.5 % shear strain at 1 Hz for 300 s; 100 % shear strain at 1 Hz for 120 s, 0.5 % shear strain at 1 Hz for 300 s, 100 % shear strain at 1 Hz for 120 s, and 0.5 % shear strain at 1 Hz for 300 s. For each composition, three replicates were evaluated.

2.4. Dressing printing, freeze-drying and crosslinking process

A SSE Regemat® Bio V1 printer (Regemat 3D, Spain) equipped with a 5 mL syringe and a 0.6 mm nozzle was used for the 3D printing of the dressings. The dressings, designed using the Regemat 3D Designer software, of 2 × 2 cm were printed in two layers with perimeter. The strand spacing was set to 1.20 mm, and the infill pattern was defined as diagonal, with a 90° deposition angle. The extrusion speed was calibrated to 9.00 mm/s. Petri dishes served as the printing platforms.

Upon completion of the printing process, the dressings were frozen at −80 °C, placed between two layers of aluminium foil, and then freeze-dried using a Lyoquest −85 freeze-dryer (Telstar, Terrassa, Spain). Freeze-dried scaffolds were transferred into glass injection vials, sealed with a rubber stopper and an aluminium crimp seal. Subsequently, a combined sterilization and crosslinking procedure was conducted at 139 °C and 1 atm for 40 min using a RAYPA AES-12 autoclave (RAYPA, Terrassa, Spain).

For the structural characterization, ($n = 5$) dressings were randomly taken from the produced set, and images were taken with an Olympus SZ-CTV stereomicroscope (Olympus, Tokyo, Japan). The dimensions were measured using ImageJ software (National Institutes of Health, Bethesda, MD, USA).

2.5. Swelling

Non-crosslinked and crosslinked dressings ($n = 3$) were weighed (*W dressing dry)* and individually placed in vials containing 5 mL of DDW or SWF, kept at 37 °C and 100 osc/min. At 0.5, 1, 4, 8, and 24 h the dressings were removed from the aqueous solution, rapidly wiped with a piece of paper and then weighed (*W dressing wet)*. The swelling percentage was calculated using Eq. (1).

$$Swelling\ \% = \frac{W\ dressing\ wet - W\ dressing\ dry}{w\ dressing\ dry} \times 100 \quad (1)$$

2.6. Mechanical properties

The mechanical properties of the dressings were assessed utilizing a TA.XT Plus Texture Analyzer (Stable Micro Systems, Surrey, UK) with a 5 kg load. Stress-strain curves were obtained at a crosshead speed of 0.1 $mm \cdot s^{-1}$. Young's modulus was determined by calculating the slope of the linear (elastic) portion of the stress-strain curve.

2.7. ATR-FTIR analysis

A direct ATR-FTIR analysis of the dressings was conducted using a Gladi-ATR (Pike Technologies, Madison, USA). Spectra were recorded in the range of 4000–400 cm^{-1}, with a resolution of 4 cm^{-1}, and averaging 64 scans per measurement to ensure an adequate signal-to-noise ratio.

2.8. Release studies

Patches were cut by half, weighed and inserted into a sealed glass vial containing 10 mL of SWF and incubated at 37 °C and 100 osc/min. At prefixed timepoints (0.5, 1, 2, 4, 6, 8, 24 h) 600 μL of the release media was taken from the vial and the absorbance was recorded at 426 nm (Agilent 8453 UV–vis spectrophotometer, Waldbronn, Germany). The released amount was calculated by means of a calibration of curve of Ber in DMSO/DDW. The experiment was conducted in triplicate.

2.9. Antimicrobial and antibiofilm tests

The antimicrobial and antibiofilm activities of the dressings were assessed against *S. aureus* (ATCC 25,923) using isothermal microcalorimetry and colony-forming units (CFUs) counting to quantify biofilm formation, similarly to previously reported methods [39]. The bacterial strain was cultured in 1 % NaCl Tryptic Soy Broth (TSB-1). The culture medium was prepared with distilled water and autoclaved at 121 °C under 1 atm pressure for 20 min. In parallel, the dressings were sterilized under crosslinking conditions at 139 °C for 40 min at 1 atm.

2.9.1. Isothermal microcalorimetry

Using previously outlined protocols, the metabolic heat of bacteria was measured using an I-Cal Flex Isothermal Calorimeter system (Calmetrix, Needham, USA), which includes eight cells, each with a 20 mL capacity. Prior to recording, the system was calibrated and stabilized at 37 °C [39,42].

To prepare the inoculum, bacteria were initially cultured on TSA plates at 37 °C for 24 h. A single bacterial colony was then selected from the plate using a sterile swab and transferred into 10 mL of broth to create a pre-inoculum, which was incubated for 24 h at 37 °C. Following incubation, 1 mL of the pre-inoculum was centrifuged in duplicate in 1.5 mL tubes at 13,000 rpm for 3 min. The supernatant was discarded, and the pellet was re-suspended in fresh broth. The optical density (O.D.) of the suspension was measured at 600 nm using a UV–vis spectrophotometer (Helios Omega, Thermofisher, Waltham, USA), and the inoculum was adjusted to achieve an O.D. of 0.1 in a 50 mL final volume.

For the calorimetric analysis, 3 mL of the bacterial inoculum was introduced into each calorimeter tube, with one dressing placed in each tube. Control tubes containing only the bacterial inoculum were also prepared.

The power, measured in milliwatts (mW), was recorded over a 24-h period to monitor energy changes associated with *S. aureus* metabolism. Data were collected at 10-second intervals for the first hour and at 1-minute intervals for the remaining time, using I-Cal Logger software. Two cells were designated for monitoring bacterial growth in media without dressings, while the other cells were used to measure the metabolic heat produced by bacteria interacting with the dressings. All experiments were conducted in duplicate, and the data were analyzed using I-Cal Reports software and visualized with GraphPad Prism.

After the microcalorimeter experiment, 100 μL of bacterial solution present in each tube was diluted 10 times using fresh broth and measured at 600 nm to quantify the O.D, in triplicate.

2.9.2. Biofilm formation quantification

After incubation in the microcalorimeter, the biofilm formation was also assessed by determining the colony-forming units (CFUs). The dressings were removed from the bacterial inoculum, transferred to 24-well plates, and subjected to three washing cycles by immersion in 2 mL of sterile PBS (pH 7.4) for 5 min to eliminate any planktonic bacteria. Subsequently, each dressing was placed in a sterile tube containing 2 mL of sterile PBS (pH 7.4), subjected to 15 min of sonication using a Branson CPX8800 Ultrasonic Cleaner (40 kHz), followed by vortexing for 30 s. The bacterial suspension in PBS (0.5 mL) was serially diluted by a factor of 10, with 4.5 mL of TSB. From each dilution, 100 μL was spread onto TSA-1 agar plates using a Digralsky spreader until the liquid was fully absorbed. This process was performed in triplicate. The plates were then incubated at 37 °C for 24 h in the dark. After incubation, the colonies were counted, and the number of CFUs per scaffold was calculated taking into account the dilution factor (df) and the total detachment volume (tdv) as described in Eq. (2).

$$\frac{CFUs}{dressing} = \frac{No.\ colonies \times df \times tdv\left(\frac{mL}{dressing}\right)}{volume\ inoculated\ on\ culture\ plate} \quad (2)$$

2.10. In vitro cytotoxicity of blank and berberine loaded dressings

Murine fibroblasts, Balb/3T3 (ATCC® CCL-163), were cultured in DMEM supplemented with 10 % FBS and 1 % antibiotic-antimycotic (growth medium), whereas human dermal fibroblasts (HDF) (ATCC® PCS-201–012) were expanded in alpha-MEM containing 10 % FBS and 1 % antibiotic-antimycotic following the manufacturer's guidelines. The culture medium was refreshed every 2–3 days and split when reaching 80 % confluency. For the assay, 40,000 cells per well were seeded in 48-well plates and allowed to adhere for 24 h. After attachment, the cell monolayers were exposed to the dressings ($n = 3$) for 24 h. The dressings were then removed, the media was discarded, and cell viability was assessed using Alamar Blue™ reagent. Non-treated cells were used as negative control whereas cells treated with pure DMSO for 5 min and then washed with PBS were used as positive control. Fresh culture medium containing 10 % Alamar Blue™ reagent was added to each well, and the plate was incubated for 2 h. After incubation, 150 μL of the supernatant was transferred to a 96-well plate, and the fluorescence intensity was measured using a plate reader (Fluostar Optima, BMG Labtech, Germany), with excitation at 540 nm and emission at 580 nm. The reagent mixture was used as blank. Cell viability was calculated by subtracting the blank signal from both the sample and the negative control (CTRL), then dividing the blank-corrected sample signal by the blank-corrected negative control signal, and multiplying the result by 100.

2.11. Statistical analysis

Statistical analysis was performed by means of GraphPad Prism (GraphPad software, La Jolla, *CA*, USA) software, using Kruskal–Wallis test followed by Dunn's post hoc test (uncorrected), and the Mann–Whitney U test. Significant differences were considered for $p < 0.05$. 0.1234 (ns), 0.0332 (*), 0.0021 (**), 0.0002 (***), <0.0001 (****).

3. Results and discussions

AMR has emerged as a major global health issue, particularly in the context of wound infections. Traditional antibiotics are becoming increasingly ineffective against resistant pathogens, urging alternative therapeutic approaches. One such strategy involves the development of wound dressings containing natural plant compounds, such as Ber, with potential antimicrobial activity [28,33,43]. An additional challenge is the creation of foldable SSE-3D printed wound dressings with pro-healing features. Current SSE-3D printing materials often struggle to combine the required flexibility with the necessary mechanical strength and biological properties needed for effective wound management. Overcoming these limitations is crucial for the development of personalized wound dressings that can better support the healing process while combating infections. To this purpose, a combination of DAC® and PVA was tested as novel ink for SSE-3D printing production of foldable dressings. Moreover, PG was added to endow the dressing with drug loading capacity.

3.1. Rheology

Firstly, the rheological profile of DAC® (1 %, 3 %, and 6 % w/v) was

investigated. DAC® 3 % showed balanced viscous and elastic properties, showing rapid recovery after intense stress. Differently, DAC® 1 % and 6 % w/v presented lower viscosity and lower recovery capability, respectively (Fig. 1**A**). Even though DAC® 3 % w/v profile was adequate for 3D printing, the final printed product did not possess the requested foldability and adaptability to the wounds. DAC®-only dressings were brittle in line with previous reports on polysaccharide-based materials [44,45].

For this reason, DAC® was mixed with a PVA solution. Indeed, PVA is biodegradable and GRAS polymer that can form transparent, strong, and flexible films [46]. Thus, it was hypothesized that when mixed with DAC® it may confer elasticity and flexibility to the final product, other than an adequate tensile strength. A solution of PVA 6.6 % was chosen based on its good balance between the capacity to be withdrawn with a syringe needle of 18 G and its viscosity. PG was added based on its ability to solubilize both water-soluble and water-insoluble compounds, allowing to load them into hydrogel-based materials [25,47]. Specifically, three ink prototypes were produced (P1, P2, P3), varying in PVA, PG, and water content. For the formulation, a "two-syringe-mixing" technique was used, as reported in methods section.

A similar rheological profile was observed for P1, P2, and P3. All inks demonstrated the initial viscosity was not fully recovered after the first compression but showed good recovery during the second (Fig. 1**B**). This behaviour suggests that once the initial viscosity barrier is overcome, the inks behave as viscoelastic liquids, making them suitable for 3D printing applications. An SSE 3D printer equipped with a piston mechanism appears optimal for this type of ink, as it allows the hydrogel to be compressed sufficiently to overcome the initial viscosity threshold before extrusion.

Among the three inks, P1 was chosen because it possesses higher PG content when compared to P2, and reduced water content when compared to P3 (Fig. 1**B**). Indeed, higher PG and lower water content can allow to load the ink with a higher concentration of natural hydrophobic compounds. In this context, Ber was selected not only for its promising antimicrobial profile, but also due to its low water solubility and the associated challenges of loading it in hydrogel-based inks. This choice was intended to demonstrate how the limitations of incorporating poorly soluble compounds into printable formulations can be effectively addressed using propylene glycol (PG) and the proposed approach. Nonetheless, during preliminary tests, we evaluated the ability of PG to solubilize a range of natural compounds and antibiotics with varying degrees of water solubility. For this purpose, we selected vancomycin (soluble), gallic acid (sparingly soluble), thymol (very slightly soluble), and Ber (insoluble) as representative compounds.

At a concentration of 5 mg/mL (highest tested), all the substances were completely solubilized in a PG/H_2O 30/70 % v/v mixture, highlighting the versatility that PG can offer for the loading of diverse therapeutic molecules (**Fig. S1**). These findings align with the well-established role of PG in pharmaceutical formulations, where it is commonly used as a co-solvent to enhance the solubility of active

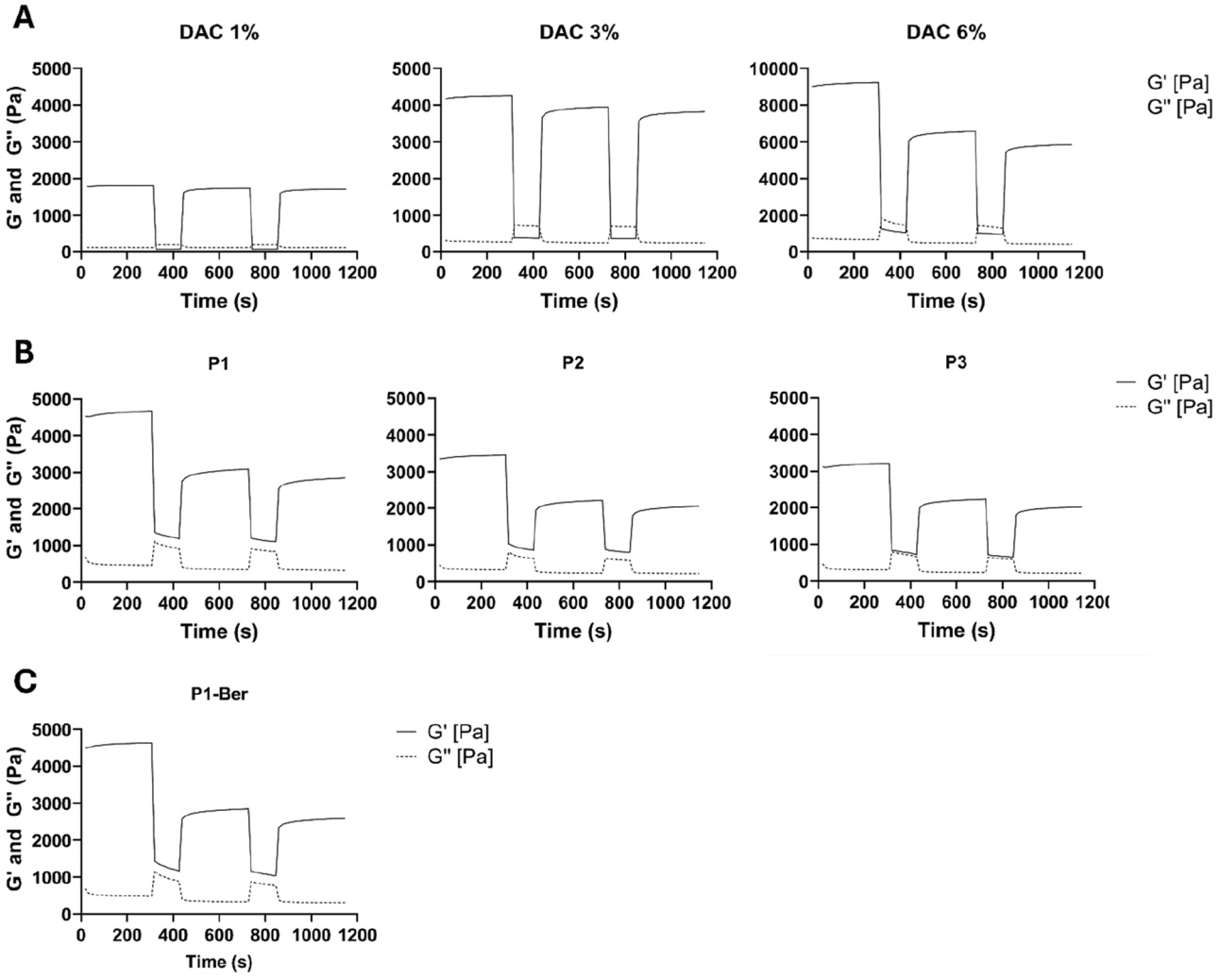

Fig. 1. A) Rheological profile of 1, 3, and 6 % w/v DAC® hydrogels; B) Rheological profile of DAC®/PVA/PG blends hydrogel: P1, P2, and P3; C) Rheological profile of Ber-loaded P1-Ber ink.

ingredients [47].

To be included into the ink, Ber was dissolved in pure PG and then mixed with the other components to obtain the final ink P1-Ber. From a rheological point of view, the addition of Ber did not modify the original ink behaviour (Fig. 1**C**).

3.2. 3D printing process and structural characterization

The P1 and P1-Ber inks were used to print porous patches of 2 × 2 cm side with perimeter and two layers. Both inks were able to produce the designed patches with good definition and resolution, maintaining the original designed structural features, as showed in Table 2. As hypothesized during rheological analysis, the piston system demonstrated to be adequate for the printing process, and the ink responded adequately to the changeable shear stress conditions.

After printing, the patches were stored at –80 °C and freeze-dried. The water removal led to a shrinking phenomenon, reducing the size of the patches from ~2 cm to ~1.5 cm side, while the pore size remained similar (Table 2 and Fig. 2). However, this step could improve the storage and chemical stability of the patches by reducing the risk of contamination associated with the presence of traces of water. Additionally, it may enable autoclave sterilization without causing melting or structural degradation. Importantly, preserving the patches in between of aluminium foil prevents premature deformation, conserving the squared and regular shape of the patch (**Fig. S2**).

In addition, as hypothesized, the DAC®/PVA/PG blend allowed to obtain patches that can be folded without giving rupture or deformation and resulting in a highly manageable product (*vide* **Video 1**).

3.3. Swelling behaviour and crosslinking

After the freeze-drying process, the ability of the patches to swell in contact with DDW and SWF was assessed (Fig. 3 and Fig. S3). The patches swelled more when immersed in DDW than in SWF probably due to the ability of Ca^{2+} ions, present in SWF, to create ionic cross-links among the carbonyl groups of DAC® chains, reducing the water uptake [48]. When immersed in DDW, the patch massively augmented its dimensions and turned into a hydrogel consistency, showing poor mechanical strength and impossibility to handle them with tweezers (Fig. S4). Conversely, when immersed in SWF, the patch augmented their dimensions but handling with tweezer was possible (Fig. S4). Nevertheless, its mechanical strength was still not adequate for medical use. To solve this problem, further reducing swelling and augmenting mechanical strength in contact with water, the patches were crosslinked in an autoclave at 139 °C for 40 min. According to previously reported data, when PVA is treated at high temperature its solubility in water massively decreases [49]. Non-heat treated PVA is hydrophilic and can readily absorb water due to its hydroxyl groups. When exposed to high temperatures, the polymer can undergo a dehydration process, which reduces its ability to form hydrogen bonds with water molecules. Moreover, the thermal degradation of PVA can lead to the breaking of polymer chains, resulting in a decrease in the polymer's molecular weight, and crystallization can occur [49]. The polymer chains can align and form ordered regions within the material, creating more rigid and less amorphous structure and leaving less volume available for water molecules to penetrate. After the crosslinking process the patches took on a more brownish colour, and the heat treatment only produced a slight shrinking of the patches (~0.1 cm).

As hypothesized, the crosslinking process reduced the swelling behaviour of the patches (Fig. 3 and Fig. S3), allowing to maintain their shape and mechanical strength in both solvents. In addition to the expected heat-induced changes in PVA, the heat could catalyze crosslinking reactions between PVA chains and the other components of the patch, further decreasing the polymer's ability to absorb water and swell.

Moreover, the UV–vis spectra of Ber released from the dressings after autoclaving confirmed the conducted heating process did not produce any degradation (Fig. S5). These data agree with previous works on the thermal stability of Ber reporting that at temperature of ~200 °C (474 K), berberine hydrochloride degradation is negligible (6/7 % of weight loss) leading H_2O [50]. Similarly, Cometa et al. observed that berberine undergoes a small initial weight loss of about 5 % below 100 °C, likely due to water or volatiles evaporation. This is followed by three main thermal events at approximately 199 °C, 392 °C, and 640 °C, which respectively correspond to melting phenomena, degradation phenomena, and the breakdown of the molecule [51].

Table 2
Dimensions of the patches after printing, after freeze-drying, and after crosslinking ($n = 3$).

Name	Length (cm)	Height (cm)	Median pore size (cm, distance between strands)
Blank-P after printing	2.13 ± 0.01	2.089 ± 0.02	0.073 ± 0.01
Ber-P after printing	2.13 ± 0.04	2.111 ± 0.02	0.086 ± 0.01
Blank-P after freeze-drying	1.54 ± 0.12	1.545 ± 0.12	0.066 ± 0.01
Ber-P after freeze-drying	1.75 ± 0.08	1.545 ± 0.12	0.082 ± 0.02
Blank-P after crosslinking	1.417 ± 0.05	1.448 ± 0.06	0.062 ± 0.01
Ber-P after crosslinking	1.433 ± 0.08	1.400 ± 0.02	0.061 ± 0.01

3.4. Mechanical properties

The tensile strength of the patches was tested before and after crosslinking and swelling in DDW. The presence of Ber decreased the Young's modulus, making it more elastic in both non-crosslinked and thermal crosslinked patches. This finding suggests that Ber may intercalate between the polymers chains and disrupt the intermolecular bonding. Conversely, the crosslinking reaction led to an increase of the Young's modulus, making the patches stiffer (Blank-P no cross *vs* Blank-P cross, and Ber-P no-cross *vs* Ber-P cross) (Fig 4**A** and Table 3). Indeed, the combination of dehydration, thermal degradation, and crosslinking process can collectively increase rigidity and stiffness, explaining the dressings behaviour [49]. In general, the behaviour of the patches showed the tendency to semi-elastically elongate during stretching phase until reaching the tear up of the mesh's filaments that compose the patches (Fig. 4**B**). The tear up phenomenon appeared to be more related to the mesh conformation and patches design than to the material composition.

3.5. ATR-FTIR

ATR-FTIR spectra of non-crosslinked patches revealed the combined characteristics of the single materials [52]. A broad -OH (DAC®+PVA) and NH (DAC®) stretch at ~3300 cm^{-1}, a peak at 1757 cm^{-1} (COO of DAC®), ~1614 cm^{-1} (amide I of DAC®), ~1138 (C–O–C ester group of DAC®), ~1080 and 1041 cm^{-1} (m C–O alcoholic and ether of DAC® and PVA) (Fig 5). Conversely, the crosslinked patches presented some slight changes which underline the modifications undergone during heat treatment. A more intense peak at 1142 cm^{-1} is present in crosslinked patches, describing an increase of the PVA crystallinity [53] (Fig 5). The increase in crystallinity can explain the higher stiffness and reduced swelling of the patches. A red shift of the -COOH stretch from 1757 to 1736 cm^{-1} was also observed, which can be common when crystallinity changes in carbohydrates [54]. Moreover, the higher intensity at 1635 cm^{-1} ($C = O$ stretching) may underline the formation of carboxylate ions due to the heat treatment and oxidation process, which explains also the brownish colour assumed by the dressings (Fig 5).

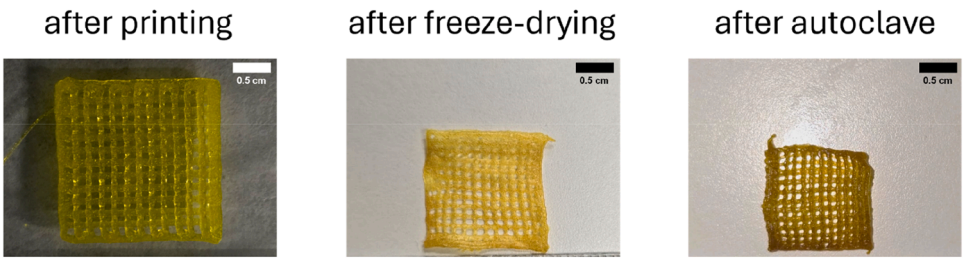

Fig. 2. Images of the patches after printing, freeze-drying, and autoclave.

3.6. Berberine release

Regarding Ber release profile, the loaded patches showed a burst release, releasing all the berberine content in the first 30 min under sink conditions (Fig. 6). This release profile can be explained by the higher affinity for water-based solvent of Ber in the presence of PG. This release profile may be suitable for antimicrobial purposes, allowing to rapidly reach the required concentration to inhibit bacterial growth. However, the *in vitro* release profile observed under sink conditions may not fully reflect the *in vivo* behaviour. Indeed, in the physiological wound environment, the release profile may depend on the volume and composition of wound exudate, which is often variable depending on the wound type and healing phase. As reported by Dealey et al. the volume of wound exudate can vary depending on the type of wound. For instance, a diabetic foot ulcer infected by Methicillin Resistant *S. aureus* (MRSA) can produce a mean of 2.8 mL/cm^2/24 h, while a bullet wound infected by *Acinetobacter* produces a mean of 1.1 mL/cm^2/24 h [55]. Thus, the morphology of the wound and the quantity of exudate can influence patches behaviour both in terms of release and efficacy. Thus, a slower and more sustained release of Ber might be observed in case of limited fluid volume diminishing the drug diffusion. Previous studies on Ber-containing wound dressings have reported similar considerations. Data reported on Ber-loaded hydrogel dressing showed fast release of Ber content within the first 6 h *in vitro* [56]. Similarly, electrospun nanofibers loaded with Ber showed a massive release of Ber content after 10 h *in vitro* [57]. Other data reports that Ber release profile is usually dependent on solvent content, solvent accessibility into the dressing matrix, and cross-linking ratio [58].

3.7. Antimicrobial and antibiofilm study

The antimicrobial and antibiofilm activity of the patches was tested against *S. aureus*, one of the most frequent pathogens in wounds infection [59,60]. Moreover, it can be used as reference to determine the antimicrobial efficacy towards Gram positive bacteria [39,61]. The results showed the presence of Ber can confer to the dressings a potent antibacterial activity, by massively decreasing the metabolic activity of *S. aureus* and its replication, in agreement with the O.D. quantification (Fig. 7). Moreover, the burst release profile of the dressing allowed to quickly counterattack the bacterial replication starting from the first hour, releasing enough Ber amount for growth inhibition. The obtained data are aligned with previous works, where *S. aureus* showed to be sensible to Ber at concentrations ranged from 32 to 128 μg/mL [29,62]. On the other hand, Ber did not improve the antibiofilm activity of the dressings towards *S. aureus* when compared to the blank dressing representing a limitation of the current formulation. Indeed, controversial data are reported in literature regarding the Ber antibiofilm performances. Tan et al. highlighted that low Ber dosage can stimulate the biofilm formation, while higher dosage can reduce it [29]. Similar findings were also reported for other staphylococci such as *S. epidermidis* [27]. A reasonable explanation may be associated to the capacity of Ber to not exert the antimicrobial efficacy directly killing, but rather, by inhibiting the replication of bacteria. Thus, bacteria that can persist in high Ber concentration environment cannot be able to replicate but are still able to form biofilms (also as a defence mechanism against Ber itself) [28]. Future strategies to enhance antibiofilm performance could include optimizing Ber dose, its combination with other antimicrobial agents, or the modification of the dressing surface to reduce biofilm adhesion.

3.8. In vitro cytotoxicity

During preliminary tests, the cytotoxicity of the blank dressing was assessed using murine Balb/3T3 fibroblasts. The data reported the presence of the blank dressing did not compromise the survival of the fibroblasts, showing no toxic effect (Fig. S6). Finally, the dressings containing Ber were tested in Human Dermal Fibroblasts (HDF), showing a decrease in cell viability associated to the Ber of ~30 % (Fig. 8). According to the ISO 10,993–5:2009 standard for the biological evaluation of medical devices, materials are considered non-cytotoxic if the reduction in cell viability is <30 % when compared to the untreated control [63]. Based on this criterion, the mean experimental values for Ber-P remained just above the threshold and did not fall into the range considered cytotoxic. This decrease in cell viability may indicate a mild stress response in fibroblasts, leading to slightly reduced proliferation, and delayed wound closure rates. However, such effects are often transient and can be *in vivo* compensated by cell migration and tissue remodelling processes.

The DAC®/PVA/PG patches developed in this work offer advantages when compared to existing dressings and platforms (Table S1). DAC® proved to be an interesting source of HA, enabling adequate 3D printing. Its rapid ability to form a hydrogel without the need for crosslinking agents or pH adjustments allows for quick ink preparation while providing viscoelastic properties [64].

Most of the polysaccharides-based SSE-3D-printed scaffolds acquire a rigid structure that cannot be folded or flexed without breaking, especially in dry state. For instance, SSE-3D printed carboxymethyl cellulose scaffolds, exhibit a rigid structure in their dry state and show only limited flexibility after swelling [65]. Similarly, Xanthan gum/guar gum-based SSE-3D-printed scaffolds acquired a sponge-like behaviour during compression after swelling, but still present limited foldability without disrupting the structure, especially in dry state [41]. Conversely, the presence of PVA in our system allowed to overcome this limitation of using polysaccharides in the production of SSE-3D-printed. A similar foldability was achieved by Yang et al. when polysaccharides were incorporated as nanofibrils, in this case formed by cellulose, produced by pressure controlled DIW [16]. Furthermore, the presence of PVA has advantages also in terms of crosslinking, avoiding the use of agents that can lead to cytotoxicity issues (e.g., glutaraldehyde vapor or photo-initiators) [66,67].

On the other hand, the use of PG as co-solvent, other than potentially allowing the encapsulation of both hydrophilic and hydrophobic compounds, allowed to include high berberine content into the ink. The accumulation of undissolved drug can produce an inconsistent nozzle blockage, impeding the correct replication of the printed object [68]. However, the used of PG can guarantee the full solubilization of active ingredient ensuring better printability and preventing nozzle clogging.

Thanks to its proven capabilities, the developed dressings can serve

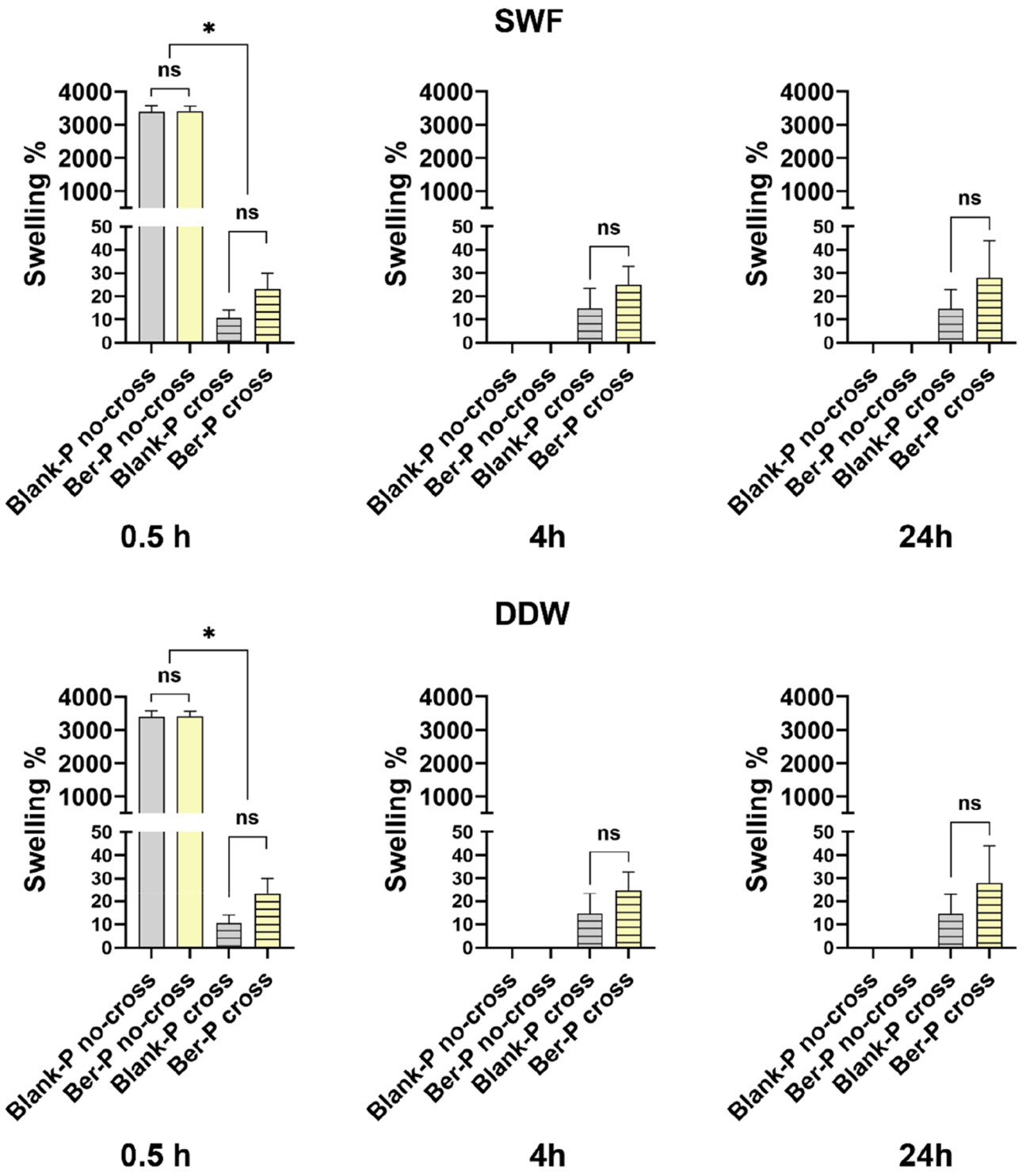

Fig. 3. Swelling profile in SWF and DDW of Blank-P and Ber-P before and after crosslinking, $n = 3$. After 1 h exposure to DDW, non-cross-linked Blank P and Ber-P were impossible to handle with tweezer and dismantled. Statistical analysis was conducted using the Kruskal–Wallis with uncorrected Dunn test and Mann–Whitney test.

as a platforms for on-demand fabrication of wound-care systems suitable for local therapies. The multifunctional properties of the developed DAC®/PVA/PG-based 3D-printed dressings suggest a possible clinical use across a broad spectrum of medical applications, particularly in areas where conventional dressings are limited. Due to their mechanical flexibility, foldability, and conformability, they are particularly well-suited for use in anatomically complex or mobile regions where conventional rigid or adhesive-based dressings are often inadequate (e.g., plantar surface, joints, perineum). Patient-specific dressing design is facilitated by the structural tunability enabled by SSE 3D printing, allowing to produce personalized dressings that precisely match the size and geometry of individual wounds. Furthermore, the demonstrated ability to incorporate both hydrophilic and hydrophobic compounds via PG could enable the loading and delivery of a wide range of therapeutic molecules, based on the patient needs. In the context of infected or high-risk wounds, the release of natural antimicrobial compounds, such as

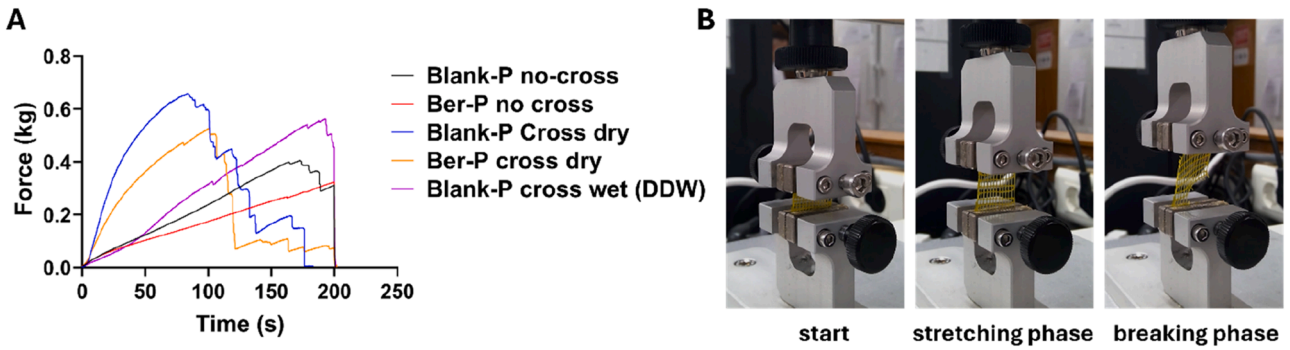

Fig. 4. A) Mechanical behaviour for dried and wet patches when subjected to stretching forces; B) Ber-P cross dry during stretching phase and breaking phase.

Table 3
Mechanical properties of patches.

Name	Young's moduli (MPa)	Tensile Strength (MPa)
Blank-P no cross	0.70	1.74
Ber-P no cross	0.50	1.41
Blank-P cross dry	1.69	2.85
Ber-P cross dry	1.35	2.05
Blank-P cross wet	1.29	1.40

Ber, may prevent infections or reduce local bacterial load, facilitating wound regeneration while fighting antimicrobial resistance (AMR).

Beyond conventional wound management, the dressing tunability and drug-loading versatility extend its potential applications also into other therapeutic domains, such as oncologic surgery [69,70]. Importantly, the dressing's compatibility with autoclave sterilization ensures its suitability for incorporation into standard clinical workflows and hospital-scale production.

4. Conclusions

The rising prevalence of AMR in wound infections calls for alternatives and the development of innovative antimicrobial wound dressing. The present study investigated the use of hyaluronic acid-based materials, specifically DAC® (a HA-g-PLA hydrogel), combined with polyvinyl alcohol (PVA) and propylene glycol (PG) to develop foldable, flexible, and non-toxic dressings incorporating antimicrobial natural compounds such as Ber.

The innovative blend of materials addresses several key challenges in wound care, particularly the need for flexible and conformable dressings that can facilitate optimal wound healing in anatomically complex areas. The rheological analysis and 3D printing of the DAC®/PVA/PG blend produced dressings with the desired printability, flexibility, and mechanical strength, showcasing the features for personalized wound care solutions that can facilitate also wound healing in anatomically complex areas.

The sterilization/crosslinking process successfully reduced the swelling behaviour of the patches and enhanced their mechanical properties. The antimicrobial and antibiofilm properties of Ber-loaded dressings were assessed, exhibiting potent antibacterial activity

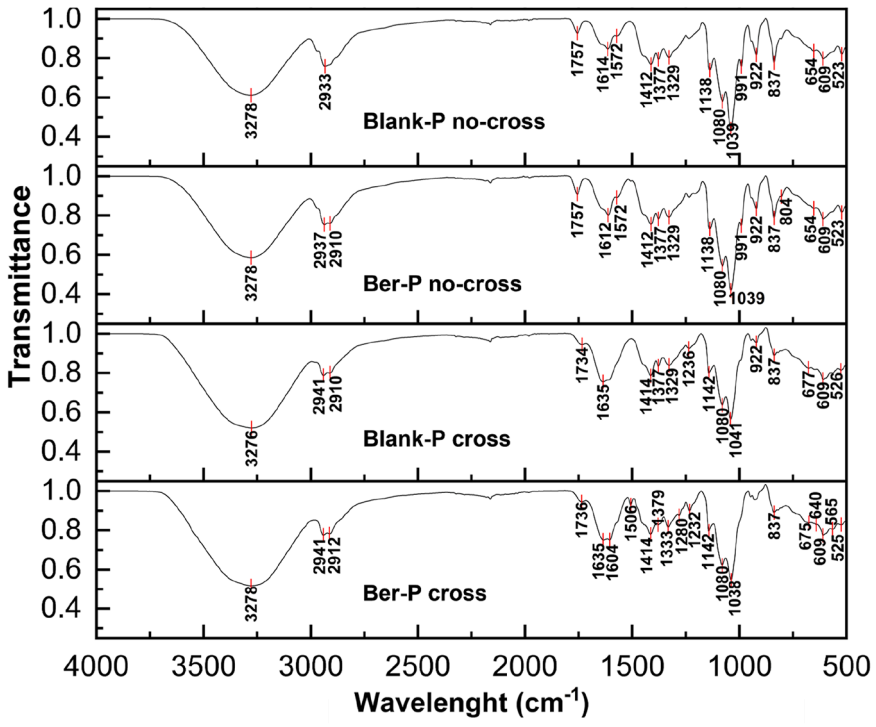

Fig. 5. ATR-FTIR spectra of Blank-P and Ber-P before and after crosslinking process. Spectra were recorded in the range of 4000–400 cm^{-1}, with 4 cm^{-1} resolution and 64 scans per measurement.

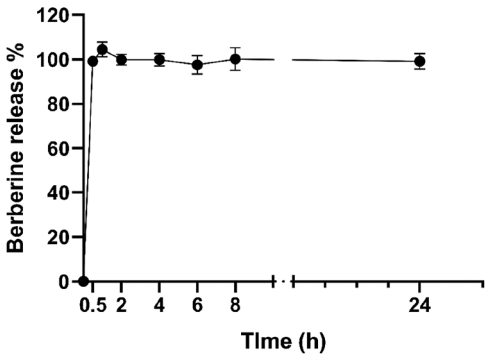

Fig. 6. Ber release profile from patches when immersed in 10 mL of SWF at 37 °C at 100 osc/min.

against *S. aureus*, a common pathogen in infected wounds. However, Ber incorporation did not significantly enhance antibiofilm activity when compared to blank patches.

Nevertheless, the use of other natural compounds (or combination of compounds) in the patches may be an interesting prospective to further enhance the antimicrobial activity of the device.

Additionally, *in vitro* cytotoxicity tests confirmed that the developed Ber-loaded dressing possesses low acute toxicity. Moreover, future studies may focus on the production process optimization, trying to avoid the shrinking phenomena of the dressing after freeze-drying and sterilization process.

Funding

The work was supported by Spain Ministerio de Ciencia, Innovación y Universidades MICIU/AEI/ 10.13039/501100011033 [PID2023-150422OB-I00], ERDF A way of making Europe, cofunded by the European Union, Xunta de Galicia [ED431C 2024/09], and Italian PON Project BONE++ Development of Micro and Nanotechnologies for Predictivity, Diagnosis, Therapy and Regenerative Treatments of Pathological Bone and Osteo-Articular Alterations [ARS01_00693]. Work partially financed by project IBEROS+ [0072_IBEROS_MAIS_1_E] Interreg-POCTEP 2021-2027.

Video 1. Ber-P after freeze-drying foldability check.

CRediT authorship contribution statement

Nicola Filippo Virzì: Writing – review & editing, Writing – original draft, Visualization, Software, Methodology, Investigation, Formal

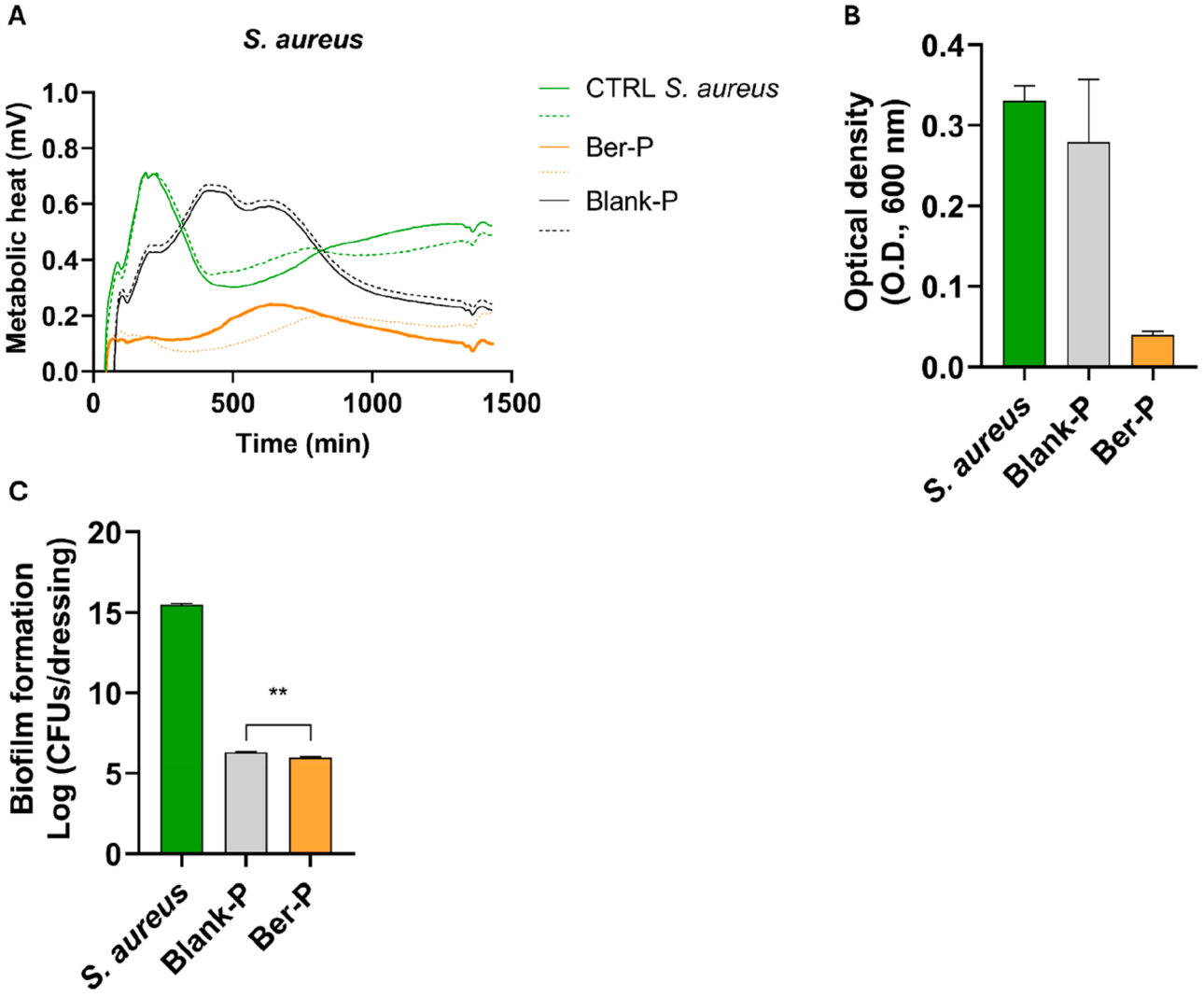

Fig. 7. Microcalorimeter graphs of Blank-P and Ber-P against *S. aureus*, O.D. quantification of planktonic bacteria, and CFUs quantification of *S. aureus* biofilms formation on patches. Two replicates for each experimental condition are indicated by solid and dotted line. Statistical analysis was conducted using the Mann–Whitney test.

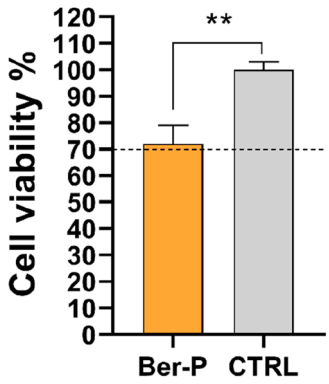

Fig. 8. *In vitro* cell viability test of HDF cells in direct contact with Ber-P for 24 h, $n = 3$. Pure DMSO was used as negative control (cell viability % 0.22 ± 0.43), while positive control (CTRL) were untreated cells. Statistical analysis was conducted using the Mann–Whitney test.

analysis, Data curation, Conceptualization. **Carmen Alvarez-Lorenzo:** Writing – review & editing, Writing – original draft, Validation, Supervision, Resources, Project administration, Methodology, Investigation, Funding acquisition, Formal analysis, Conceptualization. **Angel Concheiro:** Writing – review & editing, Visualization, Validation, Supervision, Project administration, Funding acquisition, Conceptualization. **Veronica Casagranda:** Writing – review & editing, Project administration. **Valeria Pittalà:** Writing – review & editing, Visualization, Validation, Supervision, Project administration, Funding acquisition, Conceptualization. **Patricia Diaz-Rodriguez:** Writing – review & editing, Writing – original draft, Validation, Supervision, Methodology, Investigation, Formal analysis, Conceptualization.

Declaration of competing interest

The authors declare the following financial interests/personal relationships which may be considered as potential competing interests:

Carmen Alvarez-Lorenzo reports financial support was provided by Spain Ministry of Science and Innovation. Carmen Alvarez-Lorenzo reports financial support was provided by Government of Galicia. Patricia Diaz-Rodriguez reports financial support was provided by Interreg Europe. Valeria Pittala reports financial support was provided by Italian PON Project BONE. Veronica Casagranda reports a relationship with Novagenit Srl that includes: employment. If there are other authors, they declare that they have no known competing financial interests or personal relationships that could have appeared to influence the work reported in this paper.

Acknowledgements

The authors wish to thank Dr. Davide Bellini for his valuable support during interactions with the company Novagenit Srl, project planning, and advice on formulation development.

Supplementary materials

Supplementary material associated with this article can be found, in the online version, at doi:10.1016/j.apmt.2025.102978.

Data availability

Data will be made available on request.

References

[1] M. Falcone, B. De Angelis, F. Pea, A. Scalise, S. Stefani, R. Tasinato, O. Zanetti, L. Dalla Paola, Challenges in the management of chronic wound infections, J. Glob. Antimicrob. Resist. 26 (2021) 140–147, https://doi.org/10.1016/j.jgar.2021.05.010.

[2] M. Dryden, M. Baguneid, C. Eckmann, S. Corman, J. Stephens, C. Solem, J. Li, C. Charbonneau, N. Baillon-Plot, S. Haider, Pathophysiology and burden of infection in patients with diabetes mellitus and peripheral vascular disease: focus on skin and soft-tissue infections, Clin. Microbiol. Infect. 21 (2015) S27–S32, https://doi.org/10.1016/j.cmi.2015.03.024. Suppl. 2.

[3] M. Farahani, A. Shafiee, Wound healing: from passive to smart dressings, Adv. Heal. Mater. 10 (16) (2021) e2100477, https://doi.org/10.1002/adhm.202100477.

[4] R. Laurano, M. Boffito, G. Ciardelli, V. Chiono, Wound dressing products: a translational investigation from the bench to the market, Eng. Regen. 3 (2) (2022) 182–200, https://doi.org/10.1016/j.engreg.2022.04.002.

[5] D.T. Uchida, M.L. Bruschi, 3D printing as a technological strategy for the personalized treatment of wound healing, AAPS PharmSciTech 24 (2023) 41, https://doi.org/10.1208/s12249-023-02503-0.

[6] A. Seijo-Rabina, S. Paramés-Estevez, A. Concheiro, A. Pérez-Muñuzuri, C. Alvarez-Lorenzo, Effect of wound dressing porosity and exudate viscosity on the exudate absorption: *in vitro* and in silico tests with 3D printed hydrogels, Int. J. Pharm. X 8 (2024) 100288, https://doi.org/10.1016/j.ijpx.2024.100288.

[7] I. Seoane-Viaño, P. Januskaite, C. Alvarez-Lorenzo, A.W. Basit, A. Goyanes, Semi-solid extrusion 3D printing in drug delivery and biomedicine: personalised solutions for healthcare challenges, J. Control. Release 332 (2021) 367–389, https://doi.org/10.1016/j.jconrel.2021.02.027.

[8] M. Zubair, A. Hussain, S. Shahzad, M. Arshad, A. Ullah, Emerging trends and challenges in polysaccharide-derived materials for wound care applications: a review, Int. J. Biol. Macromol. 270 (Pt 1) (2024) 132048, https://doi.org/10.1016/j.ijbiomac.2024.132048.

[9] M. Pita-Vilar, A. Concheiro, C. Alvarez-Lorenzo, L. Diaz-Gomez, Recent advances in 3D-printed cellulose-based wound dressings: a review on *in vitro* and *in vivo* achievements, Carbohydr. Polym. 321 (2023) 121298, https://doi.org/10.1016/j.carbpol.2023.121298.

[10] X. Zhou, X. Yu, T. You, B. Zhao, L. Dong, C. Huang, X. Zhou, M. Xing, W. Qian, G. Luo, 3D printing-based hydrogel dressings for wound healing, Adv. Sci. (Weinh.) 11 (47) (2024) e2404580, https://doi.org/10.1002/advs.202404580.

[11] C. Ma, L. Du, Y. Guo, X. Yang, A review of polysaccharide hydrogels as materials for skin repair and wound dressing: construction, functionalization and challenges, Int. J. Biol. Macromol. 280 (Pt 3) (2024) 135838, https://doi.org/10.1016/j.ijbiomac.2024.135838.

[12] Y. Zhao, B. Li, C. Li, Y. Xu, Y. Luo, D. Liang, C. Huang, Comprehensive review of polysaccharide-based materials in edible packaging: a sustainable approach, Foods 10 (8) (2021) 1845, https://doi.org/10.3390/foods10081845.

[13] C. Xu, G. Dai, Y. Hong, Recent advances in high-strength and elastic hydrogels for 3D printing in biomedical applications, Acta Biomater. 1 95 (2019) 50–59, https://doi.org/10.1016/j.actbio.2019.05.032.

[14] X. Li, H. Wang, D. Li, S. Long, G. Zhang, Z. Wu, Dual ionically cross-linked double-network hydrogels with high strength, toughness, swelling resistance, and improved 3D printing processability, ACS Appl. Mater. Interfaces 10 (37) (2018) 31198–31207, https://doi.org/10.1021/acsami.8b13038.

[15] J. Leppiniemi, P. Lahtinen, A. Paajanen, R. Mahlberg, S. Metsä-Kortelainen, T. Pinomaa, H. Pajari, I. Vikholm-Lundin, P. Pursula, V.P. Hytönen, 3D-Printable bioactivated nanocellulose-alginate hydrogels, ACS Appl. Mater. Interfaces 5 9 (26) (2017) 21959–21970, https://doi.org/10.1021/acsami.7b02756.

[16] Y. Yang, D. Li, N. Yan, F. Guo, A new 3D-printing strategy by enhancing shear-induced alignment of gelled nanomaterial inks resulting in stronger and ductile cellulose films, Carbohydr. Polym. 340 (2024) 122269, https://doi.org/10.1016/j.carbpol.2024.122269.

[17] S. Radmanesh, S. Shabangiz, N. Koupaei, S.A. Hassanzadeh-Tabrizi, 3D-printed biopolymeric materials as a new perspective for wound dressing and skin tissue engineering applications: a review, J. Polym. Res. 29 (2022), https://doi.org/10.1007/s10965-022-02899-6.

[18] A.R.C. Salih, H.M.U. Farooqi, H. Amin, P.R. Karn, N. Meghani, S. Nagendran, Hyaluronic acid: comprehensive review of a multifunctional biopolymer, Futur. J. Pharm. Sci. 10 (2024) 63, https://doi.org/10.1186/s43094-024-00636-y.

[19] M. Dovedytis, Z. Liu, S. Bartlett, Hyaluronic acid and its biomedical applications: a review, Eng. Regen. 1 (2020) 102–113, https://doi.org/10.1016/j.engreg.2020.10.001.

[20] Y. Kawano, V. Patrulea, E. Sublet, G. Borchard, T. Iyoda, R. Kageyama, A. Morita, S. Seino, H. Yoshida, O. Jordan, T. Hanawa, Wound healing promotion by hyaluronic acid: effect of molecular weight on gene expression and *in vivo* wound closure, Pharmaceuticals 14 (4) (2021) 301, https://doi.org/10.3390/ph14040301.

[21] M. Antoszewska, E.M. Sokolewicz, W. Barańska-Rybak, Wide use of hyaluronic acid in the process of wound healing—A rapid review, Sci. Pharm. 92 (2) (2024) 23, https://doi.org/10.3390/scipharm92020023.

[22] W. Chang, L. Chen, K. Chen, The bioengineering application of hyaluronic acid in tissue regeneration and repair, Int. J. Biol. Macromol. 270 (Pt 2) (2024) 132454, https://doi.org/10.1016/j.ijbiomac.2024.132454.

[23] G. Giammona, G. Pitarresi, F. Palumbo, C.L. Romano, E. Meani, E. Cremascoli, Hyaluronic acid-based hydrogel and use thereof in surgery, US9283283B2, Google Patents (2016). Available at, https://patents.google.com/patent/US9283283B2/en. *accessed 13 Aug 2025*.

[24] C.L. Romanò, K. Malizos, N. Capuano, R. Mezzoprete, M. D'Arienzo, C.V. Der, S. Scarponi, L. Drago, Does an antibiotic-loaded hydrogel coating reduce early post-surgical infection after joint arthroplasty? J. Bone Jt. Infect. 1 (1) (2016) 34–41, https://doi.org/10.7150/jbji.15986.

[25] N. Burduja, N.F. Virzì, G. Nocito, G. Ginestra, M.G. Saita, F. Spitaleri, S. Patanè, A. Nostro, V. Pittalà, A. Mazzaglia, Curcumin-laden hydrogel coating medical device for periprosthetic joint infection prevention and control, Int. J. Pharm. 672 (2025) 125283, https://doi.org/10.1016/j.ijpharm.2025.125283.

[26] N. Chousidis, Polyvinyl alcohol (PVA)-based films: insights from crosslinking and plasticizer incorporation, Eng. Res. Express 6 (2024) 025010, https://doi.org/10.1088/2631-8695/ad4cb4.

[27] N. Virzì, V. Greco, S. Stracquadanio, A. Jasim, K. Greish, P. Diaz-Rodriguez, N. Rotondo, S. Stefani, V. Pittalà, A. Giuffrida, Berberine-styrene-co-maleic acid nanomicelles: unlocking opportunities for the treatment and prevention of bacterial infections, RSC Adv. 14 (2024) 34066–34080, https://doi.org/10.1039/D4RA04457F.

[28] J. Tan, J. Wang, C. Yang, C. Zhu, G. Guo, J. Tang, H. Shen, Antimicrobial characteristics of berberine against prosthetic joint infection-related *Staphylococcus aureus* of different multi-locus sequence types, BMC Complement. Altern. Med. 19 (1) (2019) 218, https://doi.org/10.1186/s12906-019-2558-9.

[29] M. Chu, M.B. Zhang, Y.C. Liu, J.R. Kang, Z.Y. Chu, K.L. Yin, L.Y. Ding, R. Ding, R. X. Xiao, Y.N. Yin, X.Y. Liu, Y.D. Wang, Role of berberine in the treatment of methicillin-resistant *Staphylococcus aureus* infections, Sci. Rep. 6 (2016) 24748, https://doi.org/10.1038/srep24748.

[30] L.N. Silva, K.R. Zimmer, A.J. Macedo, D.S. Trentin, Plant natural products targeting bacterial virulence factors, Chem. Rev. 116 (16) (2016) 9162–9236, https://doi.org/10.1021/acs.chemrev.6b00184.

[31] Y. Yan, X. Li, C. Zhang, L. Lv, B. Gao, M. Li, Research progress on antibacterial activities and mechanisms of natural alkaloids: a review, Antibiotics 10 (3) (2021) 318, https://doi.org/10.3390/antibiotics10030318.

[32] W.C. Reygaert, An overview of the antimicrobial resistance mechanisms of bacteria, AIMS Microbiol. 4 (3) (2018) 482–501, https://doi.org/10.3934/microbiol.2018.3.482.

[33] R.D. Wojtyczka, A. Dziedzic, M. Kępa, R. Kubina, A. Kabała-Dzik, T. Mularz, D. Idzik, Berberine enhances the antibacterial activity of selected antibiotics against coagulase-negative *Staphylococcus* strains *in vitro*, Molecules 19 (5) (2014) 6583–6596, https://doi.org/10.3390/molecules19056583.

[34] A. Shehzad, S. Islam, E. Al-Suhaimi, Y.-S. Lee, Pleiotropic effects of bioactive phytochemicals (polyphenols and terpenes) (2018).

[35] B. Xie, Y. Liu, X. Li, P. Yang, W. He, Solubilization techniques used for poorly water-soluble drugs, Acta Pharm. Sin. B 14 (11) (2024) 4683–4716, https://doi.org/10.1016/j.apsb.2024.08.027.

[36] I. Malczak, A. Gajda, Interactions of naturally occurring compounds with antimicrobials, J. Pharm. Anal. 13 (12) (2023) 1452–1470, https://doi.org/10.1016/j.jpha.2023.09.014.

[37] M. Imenshahidi, H. Hosseinzadeh, *Berberis vulgaris* and berberine: an update review, Phytother. Res. 30 (11) (2016) 1745–1764, https://doi.org/10.1002/ptr.5693.

[38] G. Giammona, G. Pitarresi, F.S. Palumbo, S. Maraldi, S. Scarponi, C.L. Romanò, Hyaluronic-based Antibacterial Hydrogel Coating for Implantable Biomaterials in Orthopedics and trauma: from Basic Research to Clinical Applications, Intech, 2018, https://doi.org/10.5772/intechopen.73203.

[39] N.F. Virzì, P. Diaz-Rodriguez, A. Concheiro, A. Otero, A. Mazzaglia, V. Pittalà, C. Alvarez-Lorenzo, Combining antibacterial and wound healing features: xanthan gum/guar gum 3D-printed scaffold tuned with hydroxypropyl-β-cyclodextrin/thymol and Zn^{2+}, Carbohydr. Polym. 351 (2025) 123069 https://doi.org/10.1016/j.carbpol.2024.123069.

[40] J. Conceição, X. Farto-Vaamonde, A. Goyanes, O. Adeoye, A. Concheiro, H. Cabral-Marques, J. Manuel, C. Alvarez-Lorenzo, Hydroxypropyl-β-cyclodextrin-based fast dissolving carbamazepine printlets prepared by semisolid extrusion 3D printing, Carbohydr. Polym. 221 (2019) 55–62, https://doi.org/10.1016/j.carbpol.2019.05.084.

[41] N. Virzì, P. Diaz-Rodriguez, A. Concheiro, V. Pittalà, C. Alvarez-Lorenzo, Xanthan gum/guar gum-based 3D-printed scaffolds for wound healing: production, characterization, and biocompatibility screening, Carbohydr. Polym. Technol. Appl. 7 (2024) 100523, https://doi.org/10.1016/j.carpta.2024.100523.

[42] X. Farto-Vaamonde, L. Diaz-Gomez, A. Parga, A. Otero, A. Concheiro, C. Alvarez-Lorenzo, Perimeter and carvacrol-loading regulate angiogenesis and biofilm growth in 3D-printed PLA scaffolds, J. Control. Release 352 (2022) 776–792, https://doi.org/10.1016/j.jconrel.2022.10.060.

[43] S. Xia, L. Ma, G. Wang, J. Yang, M. Zhang, X. Wang, J. Su, M. Xie, *In vitro* antimicrobial activity and the mechanism of berberine against methicillin-resistant *Staphylococcus aureus* isolated from bloodstream infection patients, Infect. Drug Resist. 15 (2022) 1933–1944, https://doi.org/10.2147/IDR.S357077.

[44] D. Sanjanwala, V. Londhe, R. Trivedi, S. Bonde, S. Sawarkar, V. Kale, V. Patravale, Polysaccharide-based hydrogels for medical devices, implants and tissue engineering: a review, Int. J. Biol. Macromol. 256 (Pt 2) (2024), https://doi.org/10.1016/j.ijbiomac.2023.128488.

[45] M.M.H. Rumon, A.A. Akib, S.D. Sarkar, M.A.R. Khan, M.M. Uddin, D. Nasrin, C. K. Roy, Polysaccharide-based hydrogels for advanced biomedical engineering applications, ACS Polym. Au. 4 (6) (2024) 463–486, https://doi.org/10.1021/acspolymersau.4c00028.

[46] D.R. Seshadri, N.D. Bianco, A.N. Radwan, C.A. Zorman, K.M. Bogie, An absorbent, flexible, transparent, and scalable substrate for wound dressings, IEEE J. Transl. Eng. Health Med. 10 (2022) 4900909, https://doi.org/10.1109/JTEHM.2022.3172847.

[47] S.H. Yalkowsky, J.T. Rubino, Solubilization by cosolvents I: organic solutes in propylene glycol–water mixtures, J. Pharm. Sci. 74 (4) (1985) 416–421, https://doi.org/10.1002/jps.2600740410.

[48] A. Bonapasta, F. Buda, P. Colombet, G.L. Guerrini, Cross-linking of poly(vinyl alcohol) chains by *Ca* ions in macro-defect-free cements, Chem. Mater. 14 (2002) 1016–1022, https://doi.org/10.1021/cm010573q.

[49] S. Sau, S. Pandit, S. Kundu, Crosslinked polyvinyl alcohol: structural, optical and mechanical properties, Surf. Interfaces 25 (2021) 101198, https://doi.org/10.1016/j.surfin.2021.101198.

[50] X.X. Cheng, Y. Lui, Y.J. Hu, Y. Liu, L.W. Li, Y.-Y. Di, X.H. Xiao, Thermal behavior and thermodynamic properties of berberine hydrochloride, J. Therm. Anal. Calorim. (2009) 97, https://doi.org/10.1007/s10973-009-0288-9.

[51] S. Cometa, C. Licini, M.A. Bonifacio, P. Mastrorilli, M. Mattioli-Belmonte, E. De Giglio, Carboxymethyl cellulose-based hydrogel film combined with berberine as an innovative tool for chronic wound management, Carbohydr. Polym. 283 (2022) 119145, https://doi.org/10.1016/j.carbpol.2022.119145.

[52] F. Palumbo, G. Pitarresi, D. Mandracchia, G. Tripodo, G. Giammona, New graft copolymers of hyaluronic acid and polylactic acid: synthesis and characterization, Carbohydr. Polym. 66 (2006) 379–385, https://doi.org/10.1016/j.carbpol.2006.03.023.

[53] B. Pizzo, F. Chiozza, F. Bernardini, Thermomechanical properties of poly(vinyl alcohol) prepared at room temperature as a function of degree of hydrolysis and aluminium addition, Polym. Degrad. Stab. 227 (2024) 110887, https://doi.org/10.1016/j.polymdegradstab.2024.110887.

[54] R.S. Tipson, Infrared Spectroscopy of carbohydrates: a Review of the Literature, National Bureau of Standards, 1968.

[55] C. Dealey, J. Cameron, M. Arrowsmith, A study comparing two objective methods of quantifying the production of wound exudate, J. Wound Care 15 (4) (2006) 149–153, https://doi.org/10.12968/jowc.2006.15.4.26897.

[56] Z. Hu, K. Zhao, X. Chen, M. Zhou, Y. Chen, X. Ye, F. Zhou, Z. Ding, B. Zhu, A berberine-loaded *Bletilla striata* polysaccharide hydrogel as a new medical dressing for diabetic wound healing, Int. J. Mol. Sci. 24 (22) (2023) 16286, https://doi.org/10.3390/ijms242216286.

[57] H. Lv, S. Wang, M. He, X. Zhu, P. He, R. Sun, Z. Jia, Z. Wang, W. Zhao, Z. Zhong, Y. Han, Electrospun SF/PHBV nanofibers loaded with berberine as a bioactive wound dressing: accelerating diabetic wound healing and alleviating hypertrophic scar, Mater. Des. 251 (2025) 113574, https://doi.org/10.1016/j.matdes.2024.113574.

[58] L.T. Le, H.T. Nguyen, L.T. Nguyen, H.Q. Tran, T.T.T. Nguyen, Berberine-loaded polylactic acid nanofiber scaffold as a drug delivery system: the relationship between chemical characteristics, drug-release behavior, and antibacterial efficiency, Beilstein J. Nanotechnol. 15 (2024) 71–82, https://doi.org/10.3762/bjnano.15.7.

[59] M.S. Almuhayawi, M.H. Alruhaili, H.S. Gattan, M.T. Alharbi, M. Nagshabandi, S. Al Jaouni, S. Selim, A. Alanazi, Y. Alruwaili, O.A. Faried, M.E. Elnosary, *Staphylococcus aureus*-induced wound infections with antimicrobial resistance, methicillin- and vancomycin-resistant: assessment of emergence and cross-sectional study, Infect. Drug Resist. 16 (2023) 5335–5346, https://doi.org/10.2147/IDR.S418681.

[60] O. Simonetti, S. Marasca, M. Candelora, G. Rizzetto, G. Radi, E. Molinelli, L. Brescini, O. Cirioni, A. Offidani, Methicillin-resistant *Staphylococcus aureus* as a cause of chronic wound infections: alternative strategies for management, AIMS Microbiol. 8 (2) (2022) 125–137, https://doi.org/10.3934/microbiol.2022011.

[61] U. von Ah, D. Wirz, A.U. Daniels, Isothermal microcalorimetry—A new method for MIC determinations: results for 12 antibiotics and reference strains of *E. coli* and *S. aureus*, BMC Microbiol. 9 (106) (2009), https://doi.org/10.1186/1471-2180-9-106.

[62] H.H. Yu, K.J. Kim, J.D. Cha, H.K. Kim, Y.E. Lee, N.Y. Choi, Y.O. You, Antimicrobial activity of berberine alone and in combination with ampicillin or oxacillin against methicillin-resistant *Staphylococcus aureus*, J. Med. Food 8 (4) (2005) 454–461, https://doi.org/10.1089/jmf.2005.8.454.

[63] International Organization for Standardization (ISO), ISO 10993-5:2009, Biological evaluation of Medical devices, Part 5: Tests for *in Vitro* Cytotoxicity, ISO, Geneva, 2009.

[64] 이.주.헌. 권동건, Preparing method of hyaluronic acid hydrogel by physical treatment. KR102226724B1, Google Patents, 2021. Available at, https://patents.google.com/patent/KR102226724B1/en. *accessed 13 Aug 2025*.

[65] L. Diaz-Gomez, I. Gonzalez-Prada, R. Millan, A.Da Silva-Candal, A. Bugallo-Casal, F. Campos, A. Concheiro, C. Alvarez-Lorenzo, 3D-printed carboxymethyl cellulose scaffolds for autologous growth factors delivery in wound healing, Carbohydr. Polym. 278 (2022) 118924, https://doi.org/10.1016/j.carbpol.2021.118924.

[66] M. Dzwonkowska-Zarzycka, A. Sionkowska, Photoinitiators for medical applications—The latest advances, Molecules 29 (16) (2024), https://doi.org/10.3390/molecules29163898.

[67] G. Mugnaini, R. Gelli, L. Mori, M. Bonini, How to cross-link gelatin: the effect of glutaraldehyde and glyceraldehyde on the hydrogel properties, ACS Appl. Polym. Mater. 5 (11) (2023), https://doi.org/10.1021/acsapm.3c01676.

[68] B. Zhang, P. Belton, X.Y. Teoh, A. Gleadall, R. Bibb, S. Qi, An investigation into the effects of ink formulations of semi-solid extrusion 3D printing on the performance of printed solid dosage forms, J. Mater. Chem. B 12 (1) (2024) 131–144, https://doi.org/10.1039/D3TB01868G.

[69] C. Bastiancich, A. Malfanti, V. Préat, R. Rahman, Rationally designed drug delivery systems for the local treatment of resected glioblastoma, Adv. Drug Deliv. Rev. 177 (2021) 113951, https://doi.org/10.1016/j.addr.2021.113951.

[70] D. Di Mascolo, I. Guerriero, C. Pesce, R. Spanò, A.L. Palange, P. Decuzzi, μMESH-enabled sustained delivery of molecular and nanoformulated drugs for glioblastoma treatment, ACS Nano 17 (15) (2023) 14572–14585, https://doi.org/10.1021/acsnano.3c01574.